Quantum Confined Stark Effect in Polar InGaN/GaN Quantum Wells of Different Widths Studied by Photoluminescence Under Hydrostatic Pressure

Tadek Suski , Grzegorz Staszczak , Witold Trzeciakowski * , Lukas Uhlig , Jannina Jacqueline Tepaß , Mateusz Hajdel , Grzegorz Muziol

Posted Date: 16 April 2026

doi: 10.20944/preprints202604.1157.v1

Keywords: InGaN quantum wells; high pressure; photoluminescence; modeling of PL spectra

 doi:10.20944/preprints202604.1157.v1

Article

Quantum Confined Stark Effect in Polar InGaN/GaN Quantum Wells of Different Widths Studied by Photoluminescence Under Hydrostatic Pressure

T. Suski [1], G. Staszczak [1], W. Trzeciakowski [1,*], L. Uhlig [2], J. Tepaß [2], M. Hajdel [1] and G. Muzioł [1]

[1] Institute of High Pressure Physics, Polish Academy of Sciences, 01-142 Warsaw, Poland

[2] Institute of Physics, Chemnitz University of Technology, 09126 Chemnitz, Germany

* Correspondence: wt@unipress.waw.pl; Tel.:+48 600249698

Abstract

Low temperature photoluminescence (PL) has been studied under hydrostatic pressure and under varying excitation powers in three samples of single $In_{0.17}Ga_{0.83}N$ quantum wells with different widths: 2.6 nm, 5.2 nm, and 10.4 nm. Transitions involving ground states were strong in the 2.6 nm well, weak in the 5.2 nm well, and absent in the 10.4 nm well. Pressure coefficients of PL lines have been used to estimate the electric field in the wells. In the widest well the field seems to be fully screened (at high excitation powers). Simulations involving Poisson and Schrodinger equations allowed to identify the experimental PL lines. Pressure evolution of the PL spectra agreed with the simulation.

Keywords: InGaN quantum wells; high pressure; photoluminescence; modeling of PL spectra

1. Introduction

InGaN/GaN quantum wells are the building blocks of optoelectronic devices operating in the blue-green spectral region. Recent successes in the design of efficient nitride emitters make it possible to achieve external quantum efficiencies approaching unity [1–3]. There are also attempts to obtain efficient devices operating in red [4,5], green [6] and UV [7,8] regions of the spectrum. The corresponding multilayer structures and devices are generally grown epitaxially along the hexagonal polar crystallographic c-direction. They are characterized by strong spontaneous and piezoelectric polarizations, the latter induced by the omnipresent lattice mismatch between the substrate and individual layers of these heterostructures. The presence of epitaxial strain leads to the appearance of a built-in electric field F_{int} [9–11]. The associated effects are expressed by the so-called Quantum Confined Stark Effect (QCSE) [12,13]. Its magnitude determining the luminescence energy shift to lower values is dependent on the internal electric field, F_{int}, and on the width of the quantum well, d.

The QCSE can cause strong changes in the band structure of polar quantum wells (QWs grown along <0001> direction) and consequently in optoelectronic devices based on them [13]. The profiles of the QWs show tilting. Electrons and holes are pushed towards the opposite edges of the QW. This results in two important effects. The first one, mentioned already above, is a reduction in the emission energy ("red shift"). The second is a strong decrease in the overlap of the electron and hole wave functions, resulting in a drastic reduction in luminescence intensity. The additional disadvantage of the presence of QCSE in the active region of nitride emitters is the sensitivity of their emission wavelength/energy to the magnitude of the applied electrical or optical excitation, i.e. to the change of the applied driving current density or laser power density. This effect is due to screening of the built-in field and results in poor control of the emitted light wavelength. Furthermore, in the case of electroluminescence, increasing the driving voltage introduces an increase of the built-in field in the light emitting diodes (LEDs) or laser diodes (LDs).

 doi:10.20944/preprints202604.1157.v1

It is worth to mention that in spite of the negative effects arising from the presence of mentioned above F_{int} in polar InGaN/GaN structures and devices there are also examples of using QCSE to improve their performance. A well-known example is the AlGaN/GaN field effect transistor with 2-dimensional electron gas of high mobility [14,15]. Another positive example is the polarization doping in UV LEDs [16,17].

To minimize the detrimental effects of the internal polarization, growing devices along the orientations that have zero or minimal polarization has been proposed (see e.g., [18]). However, it should be noted that until recently, all attempts to construct highly efficient optoelectronic devices on such non-polar or semipolar directions of epitaxial growth have failed. The reason is the poor crystallographic quality of such structures and devices.

In commercial LEDs and LDs, the common range of QW width is 2-3 nm. Such narrow QWs enable to maintain high resulting electron and hole wave function overlap and thus reasonable electroluminescence intensity [19,20].

For several years now, there has been information about attempts to reduce the polarization caused effects by using wider InGaN/GaN QWs [21,22]. Apart from academic studies this solution has also been tested by the industry [21,24]. It was shown that radiative recombination in LEDs with 5 nm and 20 nm wide QWs is strong and for the most part originates from excited quantum well states.

In the present work, we focus on the studies of the photoluminescence generated in the QW structures representing the following three cases: narrow (2.6 nm), intermediate (5.2 nm), and thick (10.4 nm) $In_{0.17}Ga_{0.83}N$/GaN QWs. We observe three corresponding regimes of photoluminescence generation. The current understanding of the operation of such quantum structures can be adopted from the results obtained from the studies of emitters (LEDs and LDs) performed earlier [13,22]. In wide QWs of 10-25 nm, low current density does not induce luminescence because the overlap of distant electron and hole wave functions is negligible. Electrons and holes are localized in opposite regions of the QW near the interfaces between QWs and QBs. The QW profile is highly tilted. These separated electrons and holes localized near the interfaces are called sometimes "dark charge" since they do not contribute to the light generation (see e.g. [25]). As the excitation intensity increases, more and more electron-hole pairs are generated, leading to the screening of the built-in polarization field and the straightening of the potential profiles. Additional carrier pairs start to occupy excited states of such wide QW with significant wavefunction overlap. Strong emission (electroluminescence or photoluminescence) involving only excited states is generated.

However, the understanding of the radiative recombination processes, i.e. determination of the contribution of particular pairs of states to the luminescence spectrum was determined only recently by theoretical simulations in structures with QW widths of 10.4 and 25 nm [26].

In the current paper we study photoluminescence in three $In_{0.17}Ga_{0.83}N$/GaN structures with single QWs of different widths. The dependence of PL spectra on laser power density is determined. It leads to the blue shift of the observed transitions due to the screening of the electric field by free carriers. On the contrary, high pressure increases the built-in electric field [27,28]. It also increases the bandgap of GaN and InGaN. The main objective of the present work is to study the effects of hydrostatic pressure applied to the samples under varying excitation powers.

2. High Pressure Study of the Electric Field in the Well

In [27], a novel high-pressure method for estimating the magnitude of the internal electric field (F_{int}) in InGaN/GaN LEDs and LDs was proposed. Pressure coefficient of electroluminescence energy (dE_{EL}/dp) was analyzed in InGaN/GaN LEDs as a function of driving current density. The application of hydrostatic pressure leads to an almost linear increase of the piezoelectric field in the quantum well (QW, as demonstrated in [27,28]. The pressure coefficient of the emission energy, i.e., dE_{EL}/dp or dE_{PL}/dp, analyzed for varying laser power density (LPD), provides insight into the evolution of F_{int}. A well-established reference point is linked to the complete elimination of F_{int} from the active region of polar nitride QWs, since in that case the pressure coefficient of E_{EL} or E_{PL} equals the pressure

 doi:10.20944/preprints202604.1157.v1

coefficient of the emission energy of bulk $In_xGa_{1-x}N$ alloy [29]. Unlike heterostructures, these bulk alloys exhibit no built-in electric field. The dependence of emission energy (E_{PL}) on external hydrostatic pressure as a function of indium content is well documented, ranging from approximately 40 meV/GPa for GaN, decreasing almost linearly to 25-27 meV/GPa for x ≥ 0.25 [29]. Comparing dE_{PL}/dp in the studied quantum wells with the pressure coefficient of $In_xGa_{(1-x)}N$ alloys (with the same indium content as the QW) provides critical information that is difficult to obtain by other means. The following analysis underpins this approach.

The transition energy in QWs, influenced by the built-in electric field, can be expressed as follows [13,29]:

$$\boldsymbol{E_L = E_G + E^e_{conf} + E^h_{conf} - eL_{QW} \times F_{int} - E_{exc}} \quad (1)$$

where E_G represents the bandgap of the QW material, E_L corresponds to E_{EL} or E_{PL}, E^e_{conf} and E^h_{conf} denote the confinement energies of electrons and holes, (measured from the lower or higher edge of the well, respectively), L_{QW} is the width of the well, F_{int} is the electric field, and E_{exc} is the exciton binding energy. Since E_G is independent of the electric field, the derivative of E_L with respect to pressure (the pressure coefficient) can be written as a sum of two terms [13,28]:

$$\boldsymbol{\frac{dE_L}{dp} = \frac{dE_G}{dp} + \frac{dE_L}{dF_{int}} \times \frac{dF_{int}}{dp}} \quad (2)$$

In this formulation, it is assumed that the pressure-induced changes in all terms of Eq. (1) (except the first one) are caused by the pressure-induced variation of the F_{int}.

The first term in Eq. (2), dE_G/dp, describes the pressure coefficient of the bandgap of alloys, which has been measured for quasi-bulk $In_xGa_{(1-x)}N$, where F_{int} is zero [29]. The second term involves the product of the change in transition energy with respect to the built-in electric field, dE_L/dF_{int} which is negative, (the transition energy decreases as the field increases), and the change in the electric field with pressure, dF_{int}/dp (which is positive and nearly constant with pressure, as shown in [28]). Consequently, this product leads to a reduction of dE_L/dp relative to dE_G/dp, a decrease that becomes more pronounced for wider quantum wells and higher indium content in the QW. In our simplified approach, we assume that even under screening, the above equation holds, though the magnitude of F_{int} is reduced (in reality, under screening, the field is non-uniform).

In cases of partial screening of the piezoelectric field within the QW, the value of dE_L/dF_{int} will be lower than that in an unscreened well, as the impact of the field on E_L is less significant at low field strengths compared to high ones. Ultimately, when the field is fully screened, the measured pressure coefficient dE_L/dp of the studied QW approaches the value of dE_G/dp. Thus, deviations in dE_L/dp from values reported for bulk InGaN can be used as an indicator of the internal electric field present in the QW [13,27].

It should be mentioned, that dE_G/dp in Eq.3 denotes the pressure coefficient of InGaN alloy lattice matched to GaN substrate. It is slightly lower than the pressure coefficient of E_G in unstrained InGaN since the compressibility of GaN is lower than InGaN, and for biaxially strained InGaN we have elongation along the c-axis. However, we checked that the differences in dE_G/dp do not exceed 0.5 meV/GPa so they are within the experimental uncertainty of this parameter (±2.5 meV/GPa).

3. Materials and Methods

3.1. Samples

The studied structures were grown by plasma-assisted molecular beam epitaxy. They were deposited on bulk GaN substrates with a 2-μm-thick GaN:Si buffer layer and 20-nm-thick $In_{0.02}Ga_{0.98}N$ barrier layers. The well and the barriers were not intentionally doped. As mentioned before, the $In_{0.17}Ga_{0.83}N$ QW widths were 2.6 nm, 5.2 nm, and 10.4 nm.

 doi:10.20944/preprints202604.1157.v1

3.2. Photoluminescence Measurements

The PL was excited with a Skylark 320NX DPSSL laser (wavelength of 320 nm, 3.87 eV). A maximum power of 50 mW on the sample surface was used on the area of 4.3×9.5 μm², therefore with an estimated maximum power density of around 114 kW/cm². Laser power density was tuned by an attenuator from a minimal to maximal value of 2W/cm² and 10^5 W/ cm², accordingly. The PL signal was detected by means of a cooled charge-coupled device (CCD) camera. PL emission is strong at low temperatures while electroluminescence disappears (in *pin* diodes) due to freezeout of Mg acceptors.

Since the excitation energy is above the bandgap od the QW barriers and of the substrate, we can expect to observe PL emission from the QW, $In_{0.02}Ga_{0.98}N$ barriers and GaN.

First we studied the PL dependence on the exciting laser power density (LPD). Measurement temperature was 20K. The second type of the PL studies involved application of hydrostatic pressure (at temperature 80K). Pressure (up to 4 GPa) was applied in the Diamond Anvil Cell [30] filled with Ar. It was calibrated with the standard ruby gauge.

The choice of three QW widths enabled to study the evolution of the radiative recombination mechanisms with changes of QW width; ~~from the ground state originating effects (QW of 2.6 nm, commonly used in the light sources) to the mechanism entirely due to the excited states (QW of 10.4nm). The use of the sample with QW of intermediate width (5.2 nm) made it possible to analyze both mechanisms tuned by the strength of the laser excitation which modifies the built in field screening~~. Application of hydrostatic pressure allows to tune two parameters of the studied structures: electric field and bandgap. The bandgap of $In_{0.17}Ga_{0.83}N$ QW shows an increase with rising pressure with the rate of about 31 meV/GPa.

4. Results

4.1. Excitation-Power Dependence of PL

Figures 1–3 show results of the PL spectra measurements on the studied QWs as a function of laser power density (LPD), at T=20K.

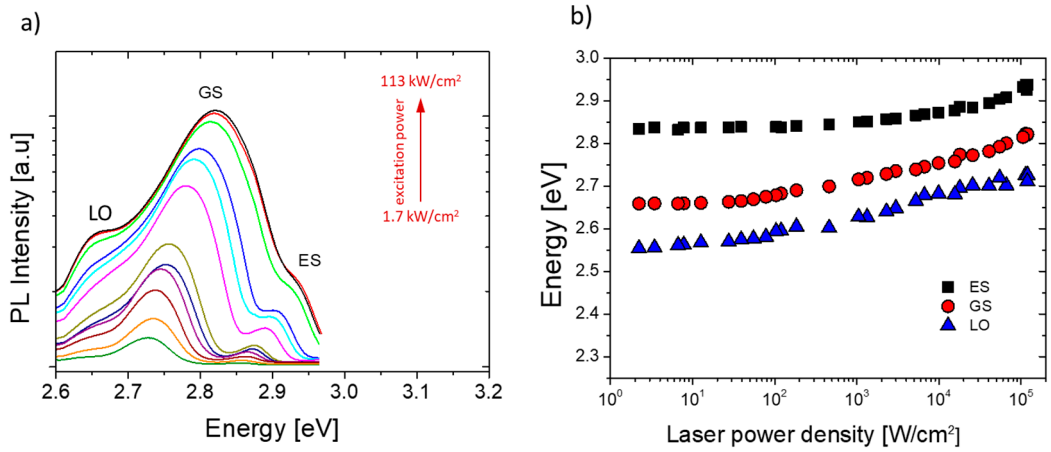

Figure 1. (a) PL spectra in log scale for different excitation LPDs (starting from 1.7 kW/cm² up till 113 kW/cm²) for sample A (2.6 nm well), (b) energy positions of three peaks versus LPD.

At the lowest LPD in Figure 1, one can observe two peaks at energies of about 2.73 and 2.87 eV. The lower energy peak (2.73 eV) is associated with the ground state radiative transition: e1-h1. The higher energy peak (2.87 eV) likely originates from the transition involving an excited state. The third peak at 2.65 eV becomes visible at higher LPDs. It is most probably the phonon replica of the main (e1-h1) transition.

With increasing LPD the two observed peaks exhibit blue-shift (Figure 1b). This behavior is due to the screening of the built-in field by electron-hole pairs introduced by the exciting laser.

 doi:10.20944/preprints202604.1157.v1

Figure 2a shows dependence of PL spectra on the LPD in the single QW sample of 5.2 nm width (sample B). Three peaks appear consecutively in the spectra with increasing LPD. The lowest energy peak is associated with (e1-h1) radiative recombination involving ground state transition. Energy of this peak exhibits strong blue-shift with increasing laser excitation (Figure 2b). At higher LPD the energy shift saturates which suggests strong reduction of the built-in field.

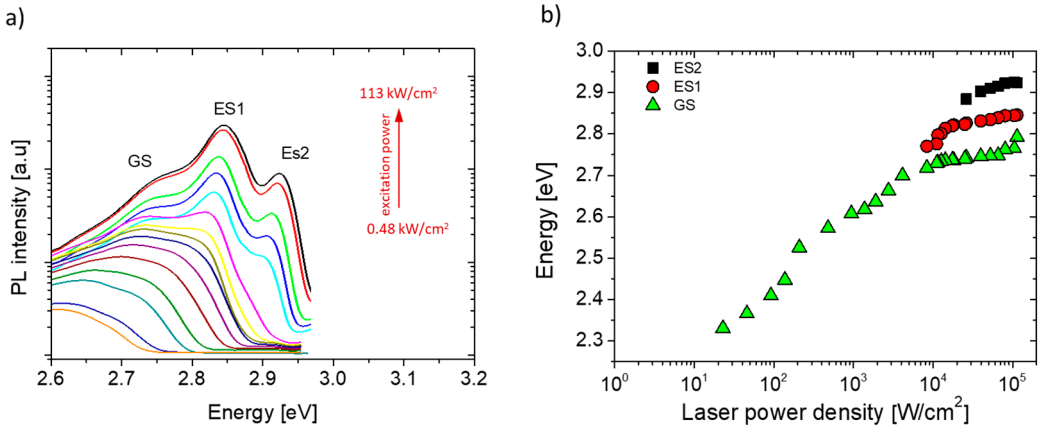

Figure 2. (a) PL spectra for different excitation LPDs (starting from 0.48 kW/cm² up till 113 kW/cm²) for sample B (5.2 nm well), (b) energy positions of three peaks versus LPD .

Positions of two higher energy peaks exhibit much less sensitivity to the excitation power (Figure 2b). We assign the origin of these peaks to the contribution of the excited states. Both PL peaks can be observed starting from a higher LPD (more efficient screening) which causes an increased wave functions overlap and increased occupation of the excited states.

Concerning the sample with 10.4 nm QW width we expect that electrons and holes generated by laser beam tend to occupy opposite regions adjacent to the interfaces of this wide QW so that for the ground states, the electron and hole wave functions overlap is negligible. Increasing the number of carriers in the ground states generated by laser beam ("dark charge") starts to screen the field in the 10.4 nm QW and above certain concentration of the injected electron-hole pairs the photoluminescence signal starts to appear. Please note that the emission appears above 1kW/cm².

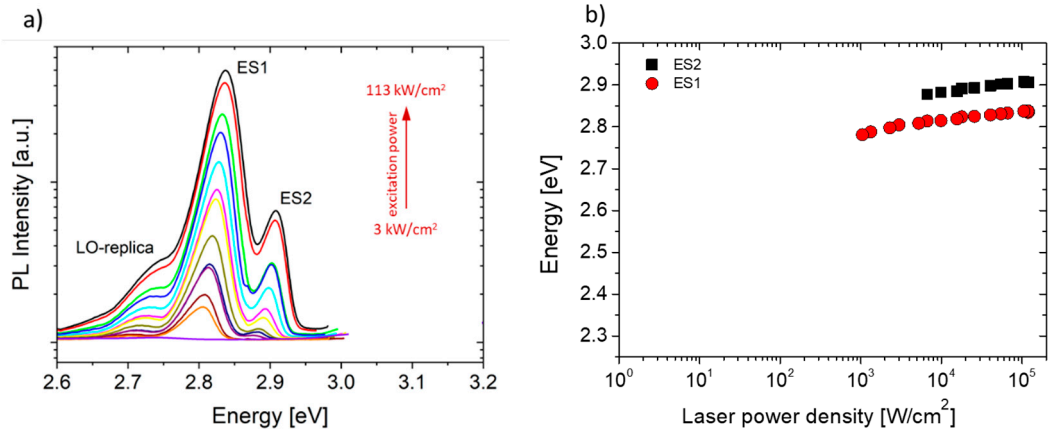

Figure 3. (a) PL spectra for different excitation LPDs (starting from 3 kW/cm² up till 113 kW/cm²) for sample C (10.4 nm well), (b) energy positions of two peaks versus LPD.

Figure 3a illustrates PL spectra originating from three radiative transitions which cover energy range between 2.6 and 3.0 eV. The lowest energy peak (with energies about 2.7-2.75 eV) is likely associated with the LO-phonon replica of the first excited state. Two peaks at about 2.8 - 2.9 eV are associated with the radiative transitions involving the excited states, ES1 and ES2 (Figure 3b).

 doi:10.20944/preprints202604.1157.v1

Energies of these two peaks are characterized by very weak increase with laser power density. It strongly suggests almost complete screening of the QCSE in this sample.

It is worth to point out that behavior of photoluminescence (studied here) and electroluminescence (see e.g. [13,22]) is similar in $In_{0.17}Ga_{0.83}N$/GaN QWs and LEDs with single QWs (in spite of the differences in the luminescence generation mechanism).

4.2. PL Under Hydrostatic Pressure at 80K

High pressure investigations of the three studied QWs of different widths were performed using diamond anvil cell (DAC) technique at 80K. The cell was filled with liquid Argon and the ruby fluorescence was used to calibrate the pressure.

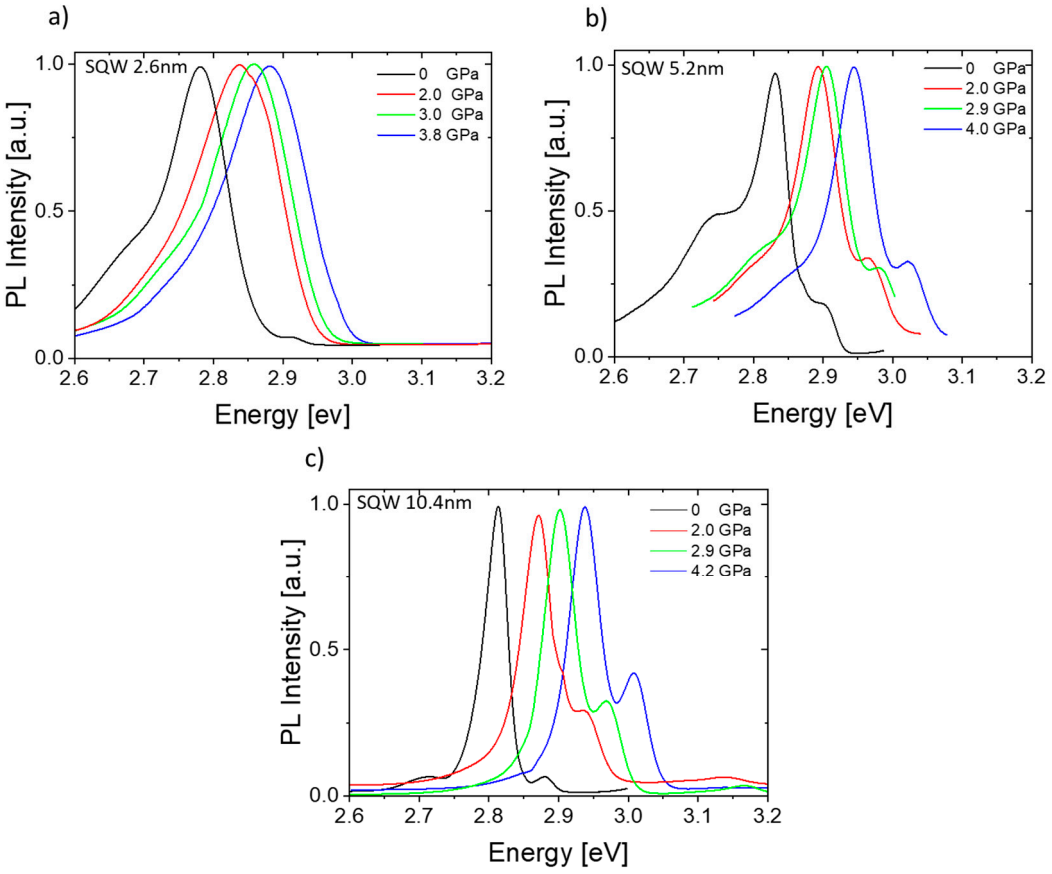

Figure 4. Pressure dependence of PL spectra for Sample A (a), Sample B (b) and Sample C (c) for the excitation power of 112 kW/cm^2.

Three sets of normalized photoluminescence spectra at increasing pressures up to about 4 GPa (at temperature 80 K) are shown in Figure 4a–c. The spectra shift to higher energies with increasing pressure. This shift is approximately linear in the applied pressure range (4 GPa), as shown in Figure 5.

 doi:10.20944/preprints202604.1157.v1

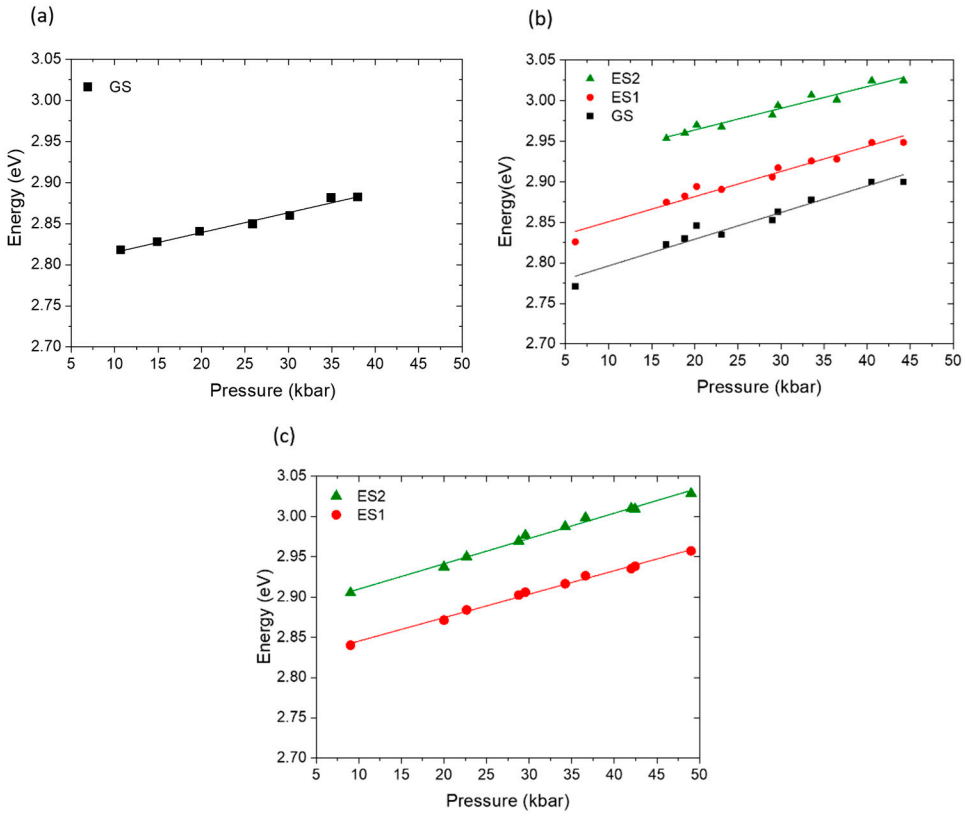

Figure 5. Pressure shift of the emission energies in Sample A (a), Sample B (b), and Sample C (c).

Similar measurements of the PL spectra versus pressure were performed for different values of excitation power density from 2 to 10^5 W/cm^2 (Figure 6).

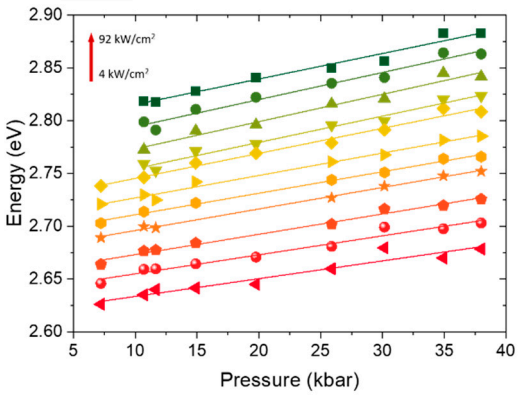

Figure 6. Pressure shift of the emission energy in Sample A for different excitation powers.

From these measurements the pressure coefficient dE_{PL}/dp has been obtained and is shown as a function of power density in Figure 7. The blue stripe covering the range between 28.5 and 33.5 meV/GPa corresponds to the bulk pressure coefficient of $In_{0.17}Ga_{0.83}N$. For the values of QW pressure coefficients in this region we can claim that the electric field vanishes (in most of the well, see Figure 8). Below this range the presence of the built-in field (increasing with pressure) lowers the pressure coefficient. The width of the blue stripe reflects the uncertainties in determination of some parameters of the $In_{0.17}Ga_{0.83}N$/GaN QW samples (e.g. the correct Indium content in the studied QW or the value of the pressure coefficient of bulk $In_{0.17}Ga_{0.83}N$).

 doi:10.20944/preprints202604.1157.v1

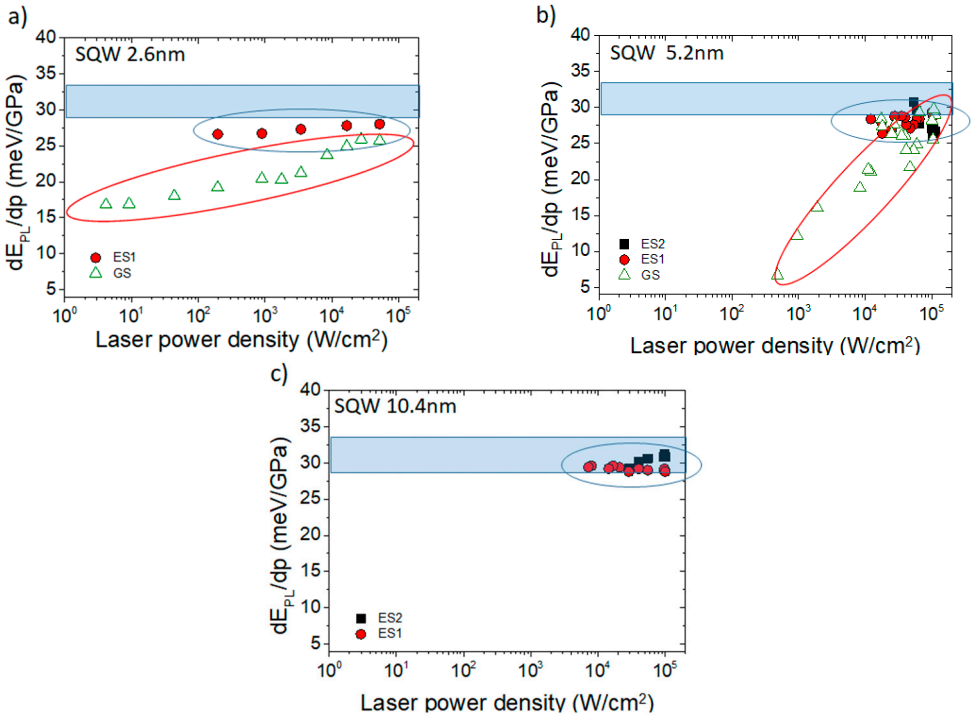

Figure 7. Pressure coefficients dE_{PL}/dp versus LPD for Sample A (a), Sample B (b), and Sample C (c).

Sample A, in the applied range of laser power density (2-10^5 W/cm^2), demonstrates the dominant contribution to photoluminescence originating from ground states (GS - green triangles). The excited state is barely visible at 80K due to broadening of the lines. Increase of dE_{PL}/dp with LPD corresponds mostly to the screening of the built-in field.

Figure 7b illustrates the evolution of the pressure coefficient of the three states observed in sample B (5.2 nm QW width). Pressure coefficient of the ground state (green triangles) increases with the applied LPD much more rapidly than in Sample A. This is because QCSE is stronger in a wider well, and the effect of screening is also stronger. The PL originating from the first and second excited states appears at two orders higher magnitude of LPD than for the ground state. It is due to the higher QCSE, i.e., lower electron-hole wave functions overlap in Sample B. The higher value of LPD increasing the number of electron-hole pairs injected into the QW creates the "dark-charge", active in screening the built-in field without generating photoluminescence, for LPD up to 5x10^2 W/cm^2. At LPD equal to about 10^4 W/cm^2 two PL peaks related to the excited states start to appear. In this LPD range, the pressure coefficients of all three observed PL peaks are slightly lower than 31 meV/GPa. It corresponds to the presence of very low built-in field.

Sample C (10.4 nm QW width) does not show PL emission related to the ground state transition e1-h1. Two excited states contribute to the PL signal at about 2.8 eV and 2.9 eV and it requires LPD higher than about 8x10^3 W/cm^2 (the first excited state) and 3x10^4 W/cm^2 (the second excited state). The resulting pressure coefficients in sample C (about 29-30 meV/GPa) show values comparable to those of bulk $In_{0.17}Ga_{0.83}N$. Thus, we can state that high pressure behavior of these radiative transitions shows that Sample C illuminated with LPD higher than about 8x10^3 W/cm^2 (within the experimental error) is characterized by the absence of built-in electric field in the central region of the well. This efficient screening of electric field is due to the presence of the sufficient concentration of "dark charge" in the QW close to the interfaces. (see Figure 8)

4.3. Simulation of the Pressure Dependence of PL Spectra

We simulate the radiative transitions in the three samples using the method described in [26] and in [31]. For a given carrier concentration, the potential profile of the quantum well is determined by self consistently solving the Poisson and Schrodinger equations, including the polarization charges and mobile charges. The valence band dispersion is described by the 6x6 kp Hamiltonian,

 doi:10.20944/preprints202604.1157.v1

and the conduction band by the spin degenerate parabolic band. The differences in effective-masses between the well and the barrier material are neglected. The model yields the dispersion of the heavy-hole band $E_{hh}(k)$, light-hole band $E_{lh}(k)$, crystal-field split-off band $E_{cf}(k)$ and the conduction band $E_c(k)$, where k is the in-plane wavevector. The wavefunctions for each band are determined in terms of the Bloch states at k=0. The carrier concentration (equal for electrons and holes) determines the positions of the Fermi levels in the conduction and in the valence bands.

The example of wavefunctions for the 10.4 nm well (Sample C) for two concentrations of injected carriers, is shown in Figure 8. At high carrier concentration the electric field in this wide well is screened, causing increased wavefunction overlap for excited states. Meanwhile, the ground states for electrons and holes remain spatially separated.

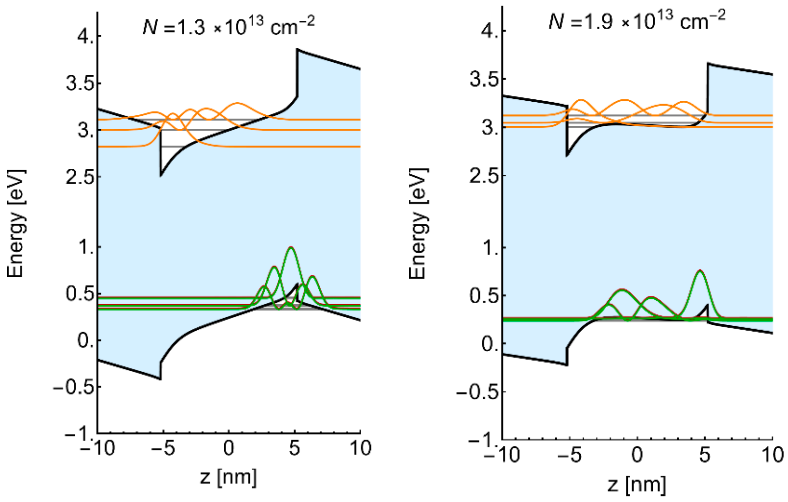

Figure 8. Wavefunctions for several bound states in the 10.4 nm QW (Sample C) at two carrier concentrations.

Having determined the energy of bound states in the well, the overlaps between valence and conduction band states $\langle e_i | h_j \rangle$ are calculated for each pair of occupied (by electrons and by holes) states. Due to the strong electric field all transitions (i,j) are allowed, their strength dependent on $\langle e_i | h_j \rangle$ and on the occupation factors. In practice, it is sufficient to consider four electronic states and ten hole states. In most cases, no higher states are confined in the QW potential. The transitions are homogeneously broadened by the parameter E_{hom}, which is estimated as 25 meV at room temperature and about 10 meV at low temperature (80 K and below). Even though the laser excitation occurs in TE mode (electric field in the plane of the well) we assume, that carriers relax to the bottom of the band with random polarization and recombine generating both TE and TM light, depending on the involved valence subband. At k=0, TE-emission arises from heavy- and light-hole bands, and TM-emission from the crystal-field split-off bands. The spontaneous emission rate $r(\hbar\omega)$ is calculated by summing up all transitions (vertical in k) between occupied conduction and valence states.

On the simulated spectra (shown further in Figures 10–13) each transition e_i-h_j is shown by a color dot: the dot height shows the transition strength (dependent on the overlap and occupation of the states), while the color represents the initial state e_i (for example, the blue color denotes transitions from e_1 to subsequent h_j states, j=1,2,3…). For example, for the narrow well (Sample A), the spectrum is dominated by the transitions from the ground state e_1; the transitions to hh_n and lh_n are so close that we denote them with the same symbol (lh1+hh1 is called h1, lh2+hh2 is called h2 etc).

The electric field in $In_xGa_{1-x}N$/GaN quantum well increases with hydrostatic pressure due to the increase of in-plane compressive strain [28]. We used the expression derived in [28] for the electric field F_x as a function of composition x and pressure p:

$$F_x(p) = (15 + 0.64p)x \tag{3}$$

where p is in GPa and the field is in MV/cm. Here we use the positive sign for pressure (it was negative in [28] to match the sign of deformation). In our case x=0.17 so the field at ambient pressure

 doi:10.20944/preprints202604.1157.v1

is about 2.5 MV/cm and it increases approximately by 0.11 MV/cm per GPa. We also have to include the pressure increase of the bandgap in $In_{0.17}Ga_{0.83}N$ which is about 31 meV/GPa. We assume that all band structure parameters do not change with pressure (except for the bandgap). An open question is the pressure dependence of carrier concentration in the well under constant illumination. We assumed, that the carrier density should increase under pressure since the field increases and the recombination rate (both radiative and non-radiative) should decrease. In order to obtain the approximate n(p) dependence, we calculated the overlap of ground state wavefunctions as a function of pressure and carrier density. Charge in the ground state is the main contributor to screening since electrons and holes are separated much more than in excited states. This is illustrated in Figure 9, where the squared overlap of the ground states is shown as a function of pressure and carrier density for the 5.2 nm well. The colors, changing from yellow through green to blue, show the decreasing overlap (i.e. recombination) for increasing pressure and for decreasing charge density.

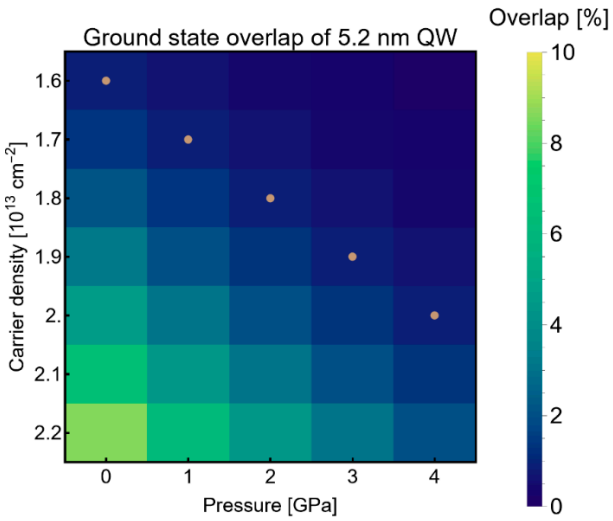

Figure 9. Squared wavefunction overlap for the ground states of electrons and holes in the 5.2 nm $In_{0.17}Ga_{0.83}N$/GaN well as a function of pressure and carrier density. The dots show the points of constant overlap $|\langle e1|h1\rangle|^2 = 0.8\%$.

Since the ambient pressure PL spectrum was fitted with $n=1.6\times10^{13}$ cm^{-2}, we calculated the corresponding overlap and kept it constant under pressure. This is shown by dots in the figure. This means the carrier density should increase from 1.6×10^{13} cm^{-2} up to 2×10^{13} cm^{-2} at the pressure of 4 GPa. Similar analysis was performed for the 2.6 nm and 10.4 nm wells. The pressure variation of concentration is shown in Table 1.

Table 1. Carrier concentration (in 10^{13} cm^{-2}) versus pressure in three samples.

Pressure [GPa]	0	1	2	3	3.8	4	4.2
Concentration in Sample A	1.4	1.453	1.505	1.558	1.6	1.611	1.621
Concentration in Sample B	1.6	1.7	1.8	1.9	1.98	2	2.02
Concentration in Sample C	1.8	1.91	2.01	2.121	2.207	2.229	2.25

4.4. Comparison with the Experiment

The concentrations from Table 1 have been used for the simulation of experimental spectra (shown for different pressures in Figures 10–12 together with the corresponding experimental spectra).

 doi:10.20944/preprints202604.1157.v1

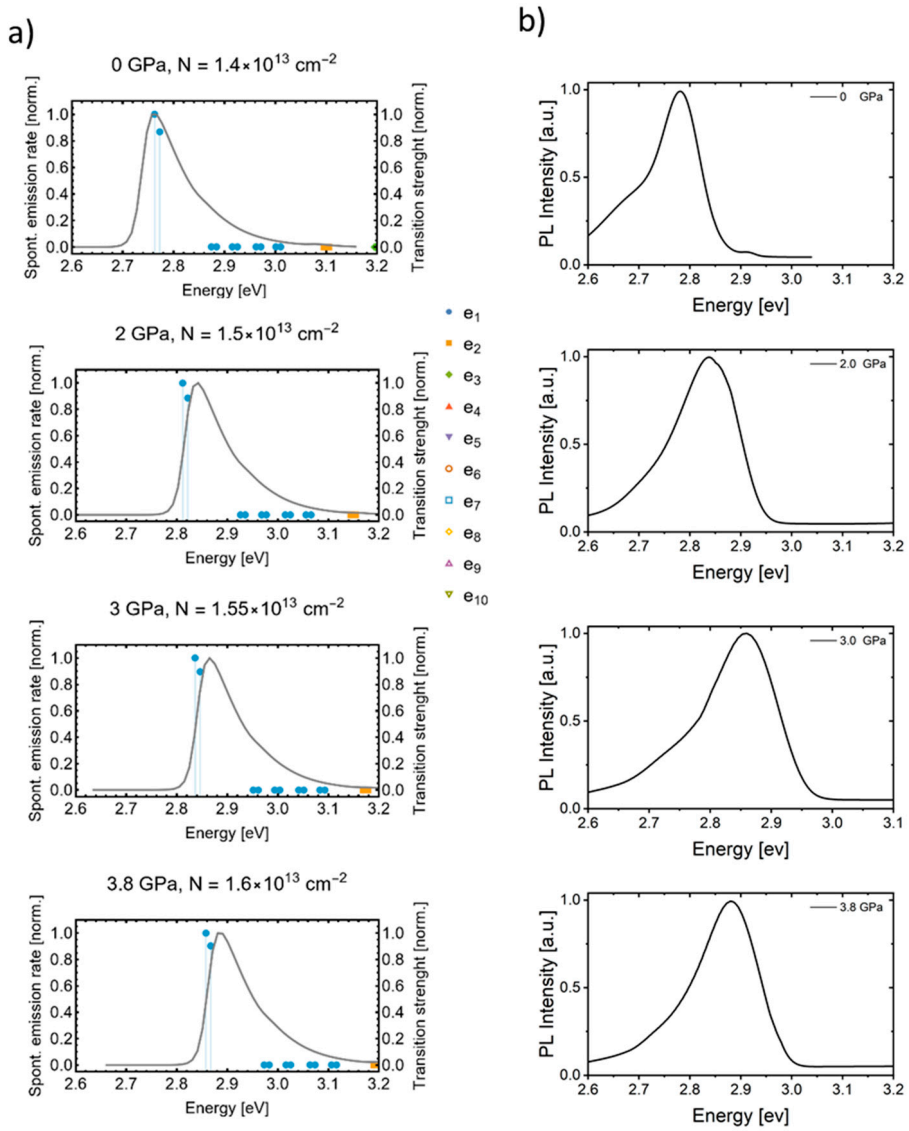

Figure 10. Theoretical spectra (a) compared to experimental spectra (b) for Sample A for selected pressures.

In Sample A the main peak is due to e1-h1 transition. The higher energy transition (e1-h2) is only observed in the experiment at ambient pressure. The experimental spectra show a low-energy tail which may be due to phonon replica.

 doi:10.20944/preprints202604.1157.v1

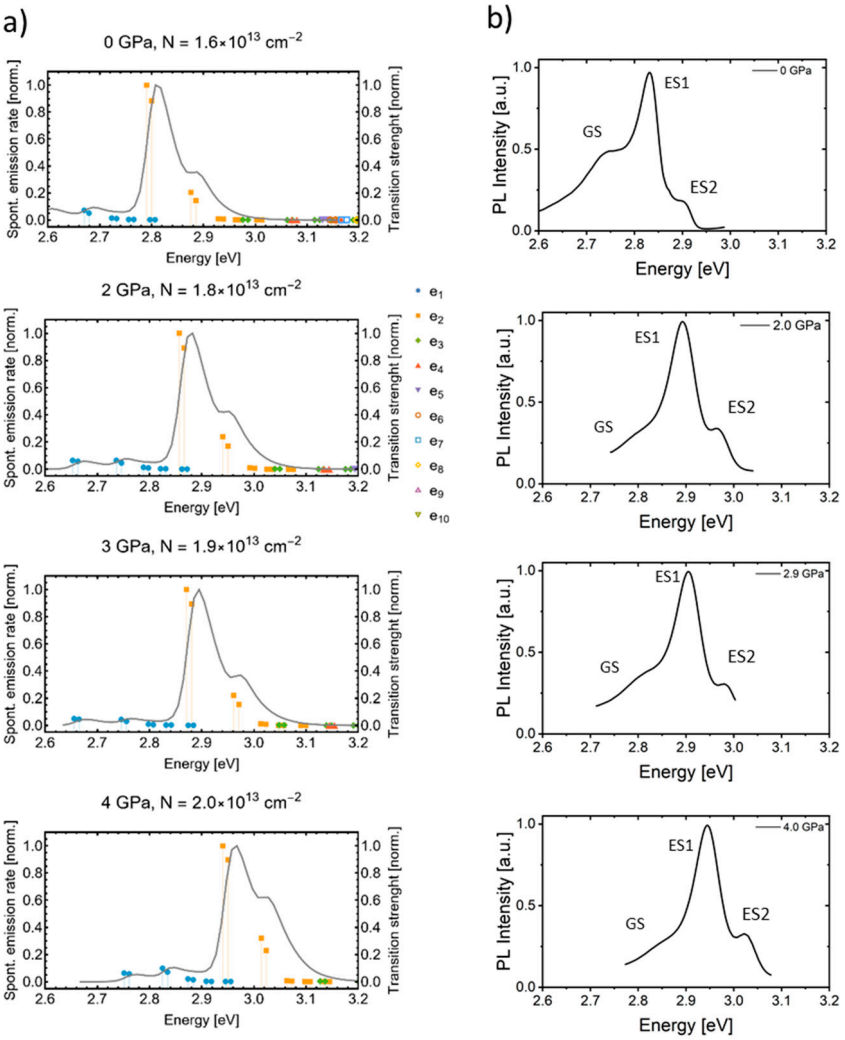

Figure 11. Theoretical spectra (a) compared to experimental spectra (b) for Sample B for selected pressures.

In Sample B the experimental spectra show a weak ground-state transition, and two excited-state transitions. The dominant peak is attributed to e2-h1 transition, and the higher-energy peak to e2-h2 transition.

 doi:10.20944/preprints202604.1157.v1

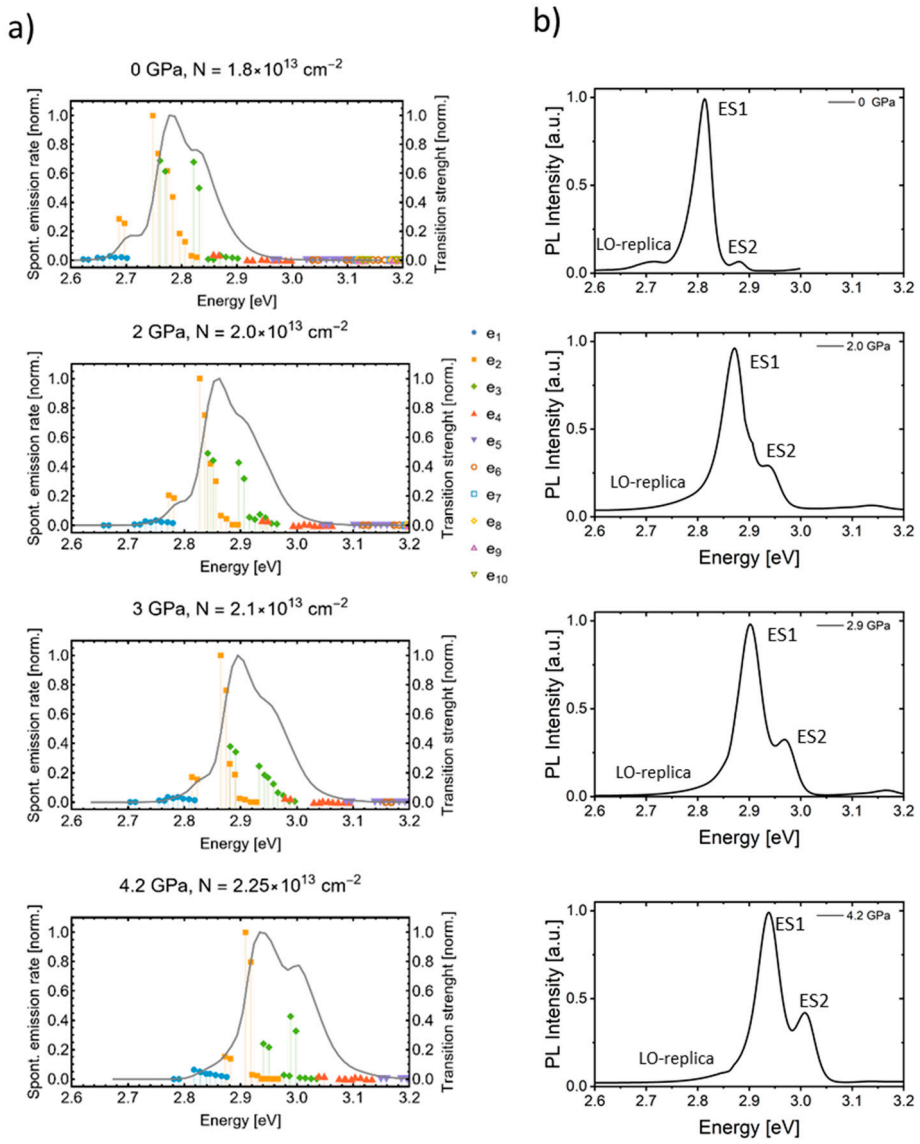

Figure 12. Theoretical spectra (a) compared to experimental spectra (b) for Sample C for selected pressures.

For Sample C we observe three peaks at low pressure (e2-h1, e2-h2 with a contribution of e3-h1, and e3-h2), and two peaks at high pressure (e2-h2 and e3-h2). The calculated spectra demonstrate that an experimental peak may be composed of several transitions. For the widest well we also note that the ground state transition (blue dots) are absent due to negligible overlap, as shown in Figure 8b. This is consistent with the idea of dark charge, which only contributes to screening of the electric field.

Finally, it is interesting to show the effect of pressure and carrier concentration in our three samples in color diagrams, displaying the value of electric field in the well as a function of these two parameters. The electric field in the middle of the well increases with pressure and decreases with increasing concentration. The red dashed line for Sample C is the zero-field limiting line, corresponding to efficient screening of the built-in field (see Figure 13). For carrier concentrations and pressures below this line the field is screened (in the middle of the well). Such "full" screening was only observed in the widest well (in the range of experimentally available LPDs). Crossing the red line represents the transition from a 2D-like system (separated eigenstates in the well) to a 3D-like system (where the excited states form a quasi-continuum). This has been analyzed in [26] as a function of carrier density; here we show that it can be done using pressure.

 doi:10.20944/preprints202604.1157.v1

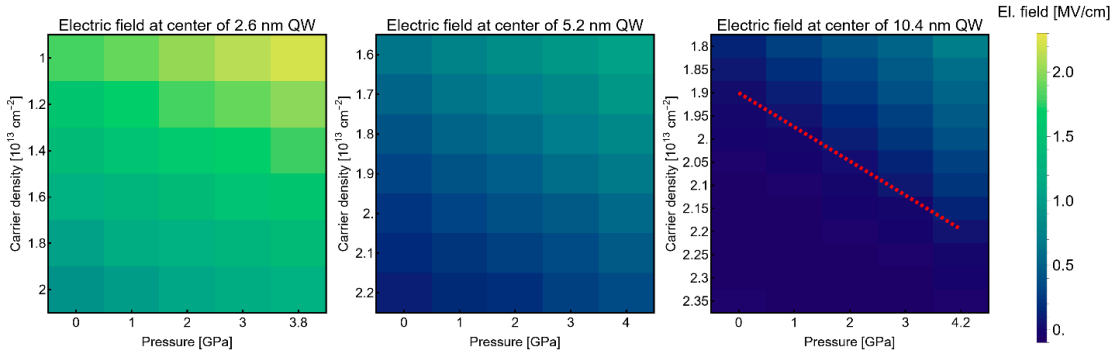

Figure 13. Color diagrams showing electric field at the center of the well for three samples as a function of carrier density and pressure. The color scale is displayed in vertical bars. Red line is a border between zero and nonzero field in the well.

4. Summary and Conclusions

We show different radiative recombination channels of single Quantum Wells of 2.6, 5.2 and 10.4 nm width. Evolution of PL energy depends strongly on the intensity of PL-exciting laser. QW of 2.6 nm shows in the entire excitation range the PL signal originating from ground and first excited states (at 20K). Energy of both states increases slowly with the increasing LPD. Screening of the built-in polarization field (responsible for this change) is not very effective in this narrow well. Pressure coefficients of the emission are much lower than for bulk $In_{0.17}Ga_{0.83}N$. The excited state transition is barely visible at 80K due to the broadening of the lines.

In 5.2 nm QW three electron-hole radiative recombination channels are involved. One observes, however, that the threshold LPDs for their appearance increases in the sequence: ground state, first excited and the second excited transition. It shows the contribution of carriers injected into the ground state, screening the built-in electric field more effectively than in the case of narrow well. Pressure coefficient of the ground state transition is low for low LPDs but becomes close to that of bulk $In_{0.17}Ga_{0.83}N$ for the highest LPDs. This implies almost full screening of the electric field at such high LDPs.

In the QW of 10.4 nm width the PL appears at the highest density of injected carriers, since it requires formation of sufficient density of "dark charge" screening the electric field. PL originates from two excited-state transitions. PL energy weakly increases with LPD. The pressure coefficients of emission lines are similar to that of bulk $In_{0.17}Ga_{0.83}N$. This demonstrates full screening of the field in the most part of the well (Figure 8).

Theoretical analysis of the effect of pressure and concentration on the band structure has been performed and good agreement with the experiment has been achieved. Simulations of emission spectra allowed to identify electron and hole states contributing to the peaks observed in the experiment.

Author Contributions: Conceptualization, T.S. and W.T.; methodology, T.S.; software, L.U. and J.T.; validation, T.S. and W.T.; investigation, G.S.; resources, G.M. and M.H.; data curation, G.S.; writing—original draft preparation, T.S.; writing—review and editing, W.T.; visualization, G.S.; supervision, W.T.; project administration, T.S.; funding acquisition, G.S. All authors have read and agreed to the published version of the manuscript.

Funding: This research was funded by the National Science Center Poland, grant number 2021/41/B/ST7/04145 and 2025/57/B/ST7/03627. For the purpose of Open Access, the author has applied a CC BY public copyright licence to any Author Accepted Manuscript (AAM) version arising from this submission.

 doi:10.20944/preprints202604.1157.v1

Data Availability Statement: Data concerning experimental results can be obtained from Grzegorz Staszczak (staszczak@unipress.waw.pl) and data concerning numerical simulations from Jannina Tepass (jannina-jacqueline.tepass@physik.tu-chemnitz.de).

Conflicts of Interest: The authors declare no conflicts of interest.

References

1. A. David, R.I. Aldaz, M.J. Cich, B. Ellis, K. Huang, F.M. Steranka, M.R. Krames, High light extraction efficiency in bulk-GaN based volumetric violet light-emitting diodes. Appl. Phys. Lett., **105**, 231111 (2014).
2. A. David, C.A. Hurni Hurni, C.A.; David, A.; Cich, M.J.; Aldaz, R.I.; Ellis, B.; Huang, K.; Tyagi, A.; DeLille, R.A.; Craven, M.D.; Steranka, F.M.; et al. Bulk GaN flip-chip violet light-emitting diodes with optimized efficiency for high-power operation. Appl. Phys. Lett. **2015**, 106, 031101.
3. Zhou, S.; Liu, X.; Yan, H.; Chen, Z.; Liu, Y.; Liu, S. Highly efficient GaN-based high-power flipchip light-emitting diodes. Opt. Express **2019**, 27, A669.
4. Yu-Ming Huang, Chun-Yen Peng, Wen-Chien Miao, Hsin Chiang, Tzu-Yi Lee, Yun-Han Chang, Konthoujam James Singh, Z. Daisuke Iida, Ray-Hua Horng, Chi-Wai Chow, Chien-Chung Lin. High-efficiency InGaN red micro-LEDs for visible light communication. Photonics Research, **10**, 1978 (2022).
5. Dong-gun Lee; Youngjin Choi; Soojin Jung; Yongmin Kim; SooYoung Park; PunJae Choi ; Sukho Yoon. High-efficiency InGaN red light-emitting diodes with external quantum efficiency of 10.5% using extended quantum well structure with AlGaN interlayers. Appl. Phys. Lett. **124**, 121109 (2024).
6. 6. H. Zhao, G. Liu, J. Zhamg, J. Dierolf, and N. Tansu, Approaches for high internal quantum efficiency green InGaN light emitting diodes with large overlap quantum wells, Opt. Express **19**(S4), A991 (2011).
7. Ziyi Zhang, Maki Kushimoto, Tadayoshi Sakai, Naoharu Sugiyama, Leo J. Schowalter, Chiaki Sasaoka and Hiroshi Amano, A 271.8 nm deep-ultraviolet laser diode for room temperature operation. Appl. Phys. Express, **12**, 124003 (2019)
8. Michael Kneissl, Tae-Yeon Seong, Jung Han and Hiroshi Amano, The emergence and prospects of deep-ultraviolet light-emitting diode technologies. *Nat. Photonics* **13**, 233–244 (2019).
9. F. Bernardini, V. Fiorentini, D. Vanderbilt, Spontaneous polarization and piezoelectric constants of III-V nitrides. Phys. Rev. B, 56, R10024–R10027. (1997).
10. 10. Tetsuya Takeuchi, Christian Wetzel, Shigeo Yamaguchi, Hiromitsu Sakai, Hiroshi Amano, and Isamu Akasaki. Determinat ion of piezoelectric fields in strained GaInN quantum wells using the quantum-confined Stark effect, Appl. Phys. Lett. **73**, 1691 (1998).
11. N. G. Young, R. M. Farrell, S. Oh, M. Cantore, F. Wu, S. Nakamura, S. P. DenBaars, C. Weisbuch, and J. S. Speck, Polarization field screening in thick (0001) InGaN/GaN single quantum well light-emitting diodes, Appl. Phys. Lett. **108**, 061105 (2016).
12. D. Miller, D.S. Chemla, T.C. Damen, A. C. Gossard, Wiegmann, T.H. Wood and C.A. Burrus. Band-Edge Electroabsorption in Quantum Well Structures: The Quantum-Confined Stark Effect. Phys. Rev. Lett. 53 (22): 2173–2176 (1984).
13. K. Pieniak, M. Chlipala, H. Turski, W. Trzeciakowski, G. Muziol, G. Staszczak, A. Kafar, I. Makarowa, E. Grzanka, S. Grzanka, C. Skierbiszewski, and T. Suski. Quantum-confined Stark effect and mechanisms of its screening in InGaN/GaN light-emitting diodes with a tunnel junction. . Opt. Express 29, 1824 (2021).
14. J. P. Ibbetson, P. T. Fini, K. D. Ness, S. P. DenBaars, J. S. Speck, and U. K. Mishra, Polarization effects, surface states, and the source of electrons in AlGaN/GaN heterostructure field effect transistors, Applied Physics Letters 77, 250 (2000)
15. Seikoh Yoshida, Hirotatsu Ishii, Jiang Li, Deliang Wang, and Masakazu Ichikawa, A high-power AlGaN/GaN heterojunction field-effect transistor, Solid-State Electronics 47, 589–592 (2003)
16. J. Simon, V. Protasenko, C. Lian, H. Xing and D. Jena, Polarization-Induced Hole Doping in Wide–Band-Gap Uniaxial Semiconductor Heterostructures. Science, **327**, 60 (2010**)**
17. L. Yan, Y. Zhang, X. Han, G. Deng, P. Li, Y. Yu, L. Chen, X. Li and J. Song, Polarization-induced hole doping in N-polar III-nitride LED grown by metalorganic chemical vapor deposition. Appl. Phys. Lett., **112**, 182104 (2018)

 doi:10.20944/preprints202604.1157.v1

18. H. Masui, S. Nakamura, S. P. DenBaars and U. K. Mishra, Nonpolar and Semipolar III-Nitride Light-Emitting Diodes: Achievements and Challenges, in *IEEE Transactions on Electron Devices*, **57**,88 (2010).
19. S. Nakamura and S. F. Chichibu, eds., *Introduction to Nitride Semiconductor Blue Lasers and Light Emitting Diodes* (CRC Press, (2014).
20. M. R. Krames, O. B. Shchekin, R. Mueller-Mach, G. O. Mueller, L. Zhou, G. Harbers, and M. G. Craford, Status and Future of High-Power Light-Emitting Diodes for Solid-State Lighting, J. Disp. Technol. **3**(2), 160–175 (2007).
21. N. F. Gardner; G. O. Müller; Y. C. Shen; G. Chen; S. Watanabe; W. Götz; M. R. Krames, Blue-emitting InGaN–GaN double-heterostructure light emitting diodes reaching maximum quantum efficiency above 200 A/cm^2, *Appl. Phys. Lett.* 91, 243506 (2007) https://doi.org/10.1063/1.2807272
22. G. Muziol, M. Hajdel, M. Siekacz, K. Szkudlarek, S. Stanczyk, H. Turski, and C. Skierbiszewski, Optical properties of III-nitride laser diodes with wide InGaN quantum wells, Appl. Phys. Express, **12**, 072003 (2019).
23. Markus Maier,_ Klaus Köhler, Michael Kunzer, Wilfried Pletschen, and Joachim Wagner, Reduced nonthermal rollover of wide-well GaInN light-emitting diodes, Appl. Phys. Lett. **94**, 041103 (2009)
24. Ansgar Laubsch, Werner Bergbauer, Matthias Sabathil, Martin Strassburg, Hans Lugauer, Matthias Peter, Tobias Meyer, Georg Brüderl, Joachim Wagner, Norbert Linder, Klaus Streubel, Berthold Hahn, Luminescence properties of thick InGaN quantum-wells. Phys. Status Solidi, **6**, S885 (2009)
25. A. Bercha, W. Trzeciakowski, G. Muziol, J. W. Tomm, and T. Suski, Evidence for "dark charge" from photoluminescence measurements in wide InGaN quantum wells, Opt. Express **31**, 3227 (2023).
26. Lukas Uhlig, Jannina Tepaß, Mateusz Hajdel, Grzegorz Muziol, and Ulrich T. Schwarz "Transition between quantum confinement and bulklike behavior in polar quantum wells, Phys. Rev. B, **108**, 045304 (2023)
27. Katarzyna Pieniak, Witold Trzeciakowski, Grzegorz Muzioł, Anna Kafar, Marcin Siekacz, Czesław Skierbiszewski, and Tadeusz Suski, „Evolution of a dominant light emission mechanism induced by changes of the quantum well width in InGaN/GaN LEDs and LDs", Optics Express, **29**, 40804 (2021).
28. W. Trzeciakowski, A. Bercha, and M. Gładysiewicz-Kudrawiec, „Hydrostatic and uniaxial effects in InGaN/GaN quantum wells", J. Appl. Phys. **124**, 205701 ((2018)
29. G. Franssen, I. Gorczyca, T. Suski, A. Kaminska, J. Pereiro, E. Muñoz, E. Iliopoulos, A. Georgakilas, S. B. Che, Y. Ishitani, A. Yoshikawa, N. E. Christensen, and A. Svane, "Bowing of the band gap pressure coefficient in $In_xGa_{1-x}N$ alloys**",** J. Appl. Phys. **103**, 033514 (2008).
30. Piotr Perlin, Izabella Grzegory, and Alain Polian, „Raman scattering and x-ray-absorption spectroscopy in gallium nitride under high pressure", Phys. Rev. B, **45**, 83 (1992).
31. W. G. Scheibenzuber, U. T. Schwarz, R. G. Veprek, B. Witzigmann, and A. Hangleiter, "Calculation of optical eigenmodes and gain in semipolar and nonpolar InGaN/GaN laser diodes" Phys. Rev. B **80**, 115320 (2009) DOI: 10.1103/PhysRevB.80.115320